



# Non-Hermitian minimal Kitaev chains

Jorge Cayao <sup>1,\*</sup> and Ramón Aguado <sup>2,†</sup>

<sup>1</sup>*Department of Physics and Astronomy, Uppsala University, Box 516, S-751 20 Uppsala, Sweden*

<sup>2</sup>*Instituto de Ciencia de Materiales de Madrid (ICMM),  
Consejo Superior de Investigaciones Científicas (CSIC),  
Sor Juana Inés de la Cruz 3, 28049 Madrid, Spain*

(Dated: June 28, 2024)

Starting from a double quantum dot realization of a minimal Kitaev chain, we demonstrate that non-Hermiticity stabilizes the so-called poor man’s Majorana zero modes in a region of parameter space that is much broader than in the Hermitian regime. In particular, we consider the simplest non-Hermitian mechanism which naturally appears due to coupling to normal reservoirs and is commonly present in all transport experiments. Specifically, such couplings induce exceptional points which connect stable and highly tunable zero energy real lines that are well separated from the quasicontinuum. Such zero-energy lines reflect spectral degeneracies protected by topology and represent the non-Hermitian generalization of the Hermitian poor mans Majorana modes occurring at single points in parameter space. Our findings pave the way for realizing robust non-Hermitian effects by combining unconventional superconductors and non-Hermitian topology.

Majorana zero modes (MZMs) have attracted an enormous interest during the past decade not only because they characterize topological superconductivity [1–3], a new state of matter, but also due to their potential use in fault tolerant quantum computation [4–6]. This topological state was predicted to appear in engineered  $p$ -wave superconductors, based on e.g. semiconductor-superconductor hybrid nanostructures [7–10].

The unambiguous detection of MZMs has been hotly debated in the last decade [11]. However, the recent experimental demonstration [12, 13] of bottom-up engineering of a Kitaev chain [14] has given new impetus to the field. These experiments confirm that a minimal Kitaev chain can be realized with only two quantum dots (QDs) coupled by a superconductor [15], see also Ref. [16]. MZMs in these minimal chains only appear in fine-tuned “sweet spots” in parameter space and without topological protection, so they are often called poor man’s Majorana modes (PMMs). Reaching such sweet spots is challenging as it involves having equal electron co-tunneling (ECT) and crossed Andreev reflection (CAR) [17], a condition that has recently been achieved using a hybrid semiconductor-superconductor segment mediating the coupling between QDs [12, 13];[18–21].

Typical experiments for detecting PMMs involve local and nonlocal conductances [12, 13]. As such, the sample is contacted by metallic leads which play the role of reservoirs, see e.g., Ref. [12]. A suitable mathematical language to describe this open quantum system is the so-called non-Hermitian (NH) formulation [22, 23]. At very weak couplings, the NH impact of the leads slightly affects the sample via a broadening of the conductance measurements [24]. In this limit, such measurements essentially reveal the spectrum of the closed quantum system. However, when the coupling to the leads is comparable to other energy scales, NH effects considerably change the properties of the isolated system and give rise

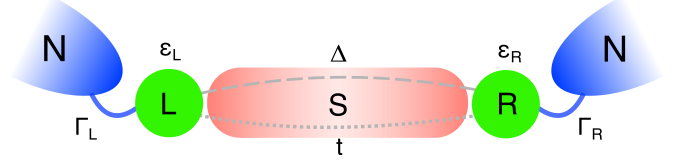


FIG. 1. A two-site Kitaev chain realized by coupling two QDs (green circles) with onsite energies  $\varepsilon_{L,R}$  through a common superconductor (red). This system hosts poor man’s Majorana modes when single ( $t$ ) and two electron ( $\Delta$ ) tunneling are equal. Coupling this minimal Kitaev chain to normal leads  $N$  (blue regions) by rates  $\Gamma_{L,R}$  makes the system non-Hermitian.

to unique phenomena that does not exist in the Hermitian regime [23, 25, 26]; see also Refs. [27–31].

In this work, we demonstrate that non-Hermiticity is a powerful mechanism to stabilize and realize PMMs through the emergence of NH spectral degeneracies known as exceptional points (EPs), where eigenvalues and eigenvectors coalesce. In particular, we consider a NH two-site Kitaev chain with non-Hermiticity due to coupling the two QDs to normal leads by  $\Gamma_{L,R}$ , see Fig. 1. We discover that, when  $\Gamma_L \neq \Gamma_R$ , EP bifurcations generate zero-energy lines where PMMs are stable beyond the Hermitian sweet spot. We further demonstrate that the emergent EPs and zero-energy lines can be detected via spectroscopy and conductance. Since EPs possess an inherent NH topology and are protected by fundamental symmetries [25, 32, 33], the zero-energy lines and NH PMMs represent topologically protected NH effects.

*NH two-site Kitaev chain.*—We consider a minimal Kitaev model where two (left/right) QDs with energies  $\varepsilon_{L/R}$  couple via a superconductor that allows for CAR and ECT [12, 15, 17], see Fig. 1. These two processes are parametrised by  $\Delta$  and  $t$ , respectively, resulting in a minimal Kitaev Hamiltonian

$$H_K = \varepsilon_L \sigma_+ \tau_z + \varepsilon_R \sigma_- \tau_z + t \sigma_x \tau_z - \Delta \sigma_y \tau_y, \quad (1)$$

where  $\sigma_{\pm} = (\sigma_0 \pm \sigma_z)/2$  and  $\sigma_i$  ( $\tau_i$ ) is the  $i$ -th Pauli matrix in the QD (Nambu) subspace.

Non-Hermiticity is introduced by coupling each QD to normal (N) leads, as in Fig. 1. The resulting open system is described by an effective NH Hamiltonian that reads

$$H_{\text{eff}} = H_K + \Sigma^r(\omega = 0), \quad (2)$$

where  $\Sigma^r(\omega = 0)$  is the zero-frequency retarded self-energy characterizing the coupling of each QD to the N leads. Since only the imaginary part of the self-energy induces NH effects [27, 34–45], we take the so-called wide limit [24] and parametrize the couplings as  $\Gamma_{L/R} = \pi|\tau|^2\rho_{L/R}$ , where  $\tau$  is the hopping amplitude and  $\rho_{L/R}$  the surface density of states of the left/right lead. This results in a purely imaginary self-energy of the form  $\Sigma^r(\omega = 0) = \text{diag}(\Sigma_{e^+}^r, \Sigma_{e^-}^r)$ , with  $\Sigma_{e^{(h)}}^r = -i\Gamma\sigma_0 - i\gamma\sigma_z$ ,  $\Gamma = (\Gamma_L + \Gamma_R)/2$  and  $\gamma = (\Gamma_L - \Gamma_R)/2$ . Next we explore the role of such NH self-energy for realizing PMMMs.

*PMMMs at the sweet spot  $\Delta = t$ .*—We begin by analyzing the impact of non-Hermiticity on the sweet spot  $\Delta = t$ , which is a single point in parameter space where PMMMs appear in the Hermitian regime [12]. To inspect the realization of PMMMs, we obtain the eigenvalues of  $H_{\text{eff}}$ . At  $\varepsilon_{L,R} = \varepsilon$ , they are given by

$$E_j^{\pm} = -i\Gamma \pm \sqrt{P - (-1)^j 2\sqrt{Q}}, \quad (3)$$

where  $P = 2t^2 + \varepsilon^2 - \gamma^2$ ,  $Q = t^2(t^2 + \varepsilon^2) - \varepsilon^2\gamma^2$ , and  $j = 0(1)$  labels the first (second) electron- and hole-like eigenvalues. At  $\varepsilon = 0$ , we get  $E_0^{\pm} = -i\Gamma \pm i|\gamma|$  and  $E_1^{\pm} = -i\Gamma \pm \sqrt{4t^2 - \gamma^2}$ . Physically, the first set of eigenvalues corresponds to PMMMs which acquire different lifetimes, while the second set are bulk modes. This implies that  $E_0^{\pm}$  has zero real (Re) part and distinct imaginary (Im) components [46]. Therefore, when  $\Delta = t$  and  $\varepsilon = 0$ , non-Hermiticity only gives finite lifetimes to the already zero-energy PMMMs. In contrast, the bulk levels  $E_1^{\pm}$ , have finite Re and Im parts, implying that there is always a gap for  $2t > |\gamma|$ . However, such gap vanishes at  $2t = |\gamma|$  when  $E_1^{\pm}$  merge into a single value. We have verified that the eigenvectors associated to  $E_1^{\pm}$  also merge, thus signalling the formation of exceptional points (EP) at  $2t = \pm|\gamma|$ . Even though such EPs due to  $E_1^{\pm}$  are inherently interesting, they are detrimental for PMMMs, since there is no gap separating the zero modes from the quasicontinuum in real samples.

The situation becomes more interesting when  $\Delta = t$  but  $\varepsilon \neq 0$ . In the Hermitian regime, the lowest energy levels develop a single zero-energy crossing at  $\varepsilon = 0$  which disperses as  $E_0^{\pm} \approx \pm\varepsilon^2/(2\Delta)$ , see gray curves in Fig. 2(a), reflecting the so-called quadratic protection [15]. Interestingly, in the NH case, the lowest energy levels  $E_0^{\pm}$ , blue curves in Fig. 2(a), can acquire zero Re part for a large range of  $\varepsilon \neq 0$  when  $0 < P \leq \text{Re}(2\sqrt{Q})$  and  $\text{Im}(2\sqrt{Q}) = 0$ , where the equality defines the formation

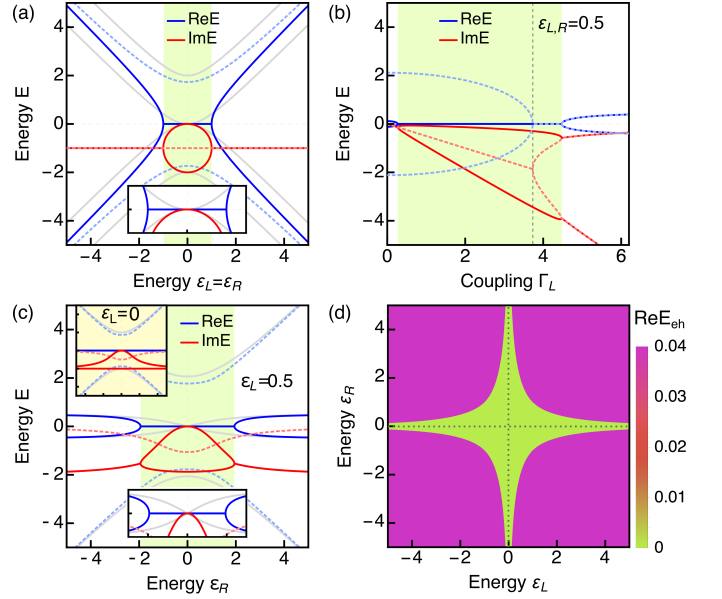


FIG. 2. Re (blue) and Im (red) parts of the eigenvalues in the sweet spot  $\Delta = t$  at finite non-Hermiticity, where dashed light colors correspond to bulk eigenvalues. Panel (a) shows the eigenvalues as a function of  $\varepsilon_L = \varepsilon_R$ , while (b,c) as a function of  $\varepsilon_R$  at  $\varepsilon_L = 0.5$ , respectively. The gray curves in (a-c) correspond to  $\Gamma_{L,R} = 0$ , while the green region ends mark the EPs due to lowest eigenvalues. Vertical dashed line in (c) mark EPs due to higher energy eigenvalues. Panel (d) shows the Re part of the difference between lowest positive and negative eigenvalues  $\text{Re}E_{eh}$ , where the green region indicates  $\text{Re}E_{eh} = 0$  and its borders mark the EPs. The dotted lines indicate in (d)  $\text{Re}E_{eh} = 0$  at  $\Gamma_{L,R} = 0$ . Parameters:  $\Delta = t = 1$ ,  $\Gamma_L = 2$ ,  $\Gamma_R = 0$ .

of EPs and the inequality ensures zero Re part between EPs. From the equality we obtain two QD energies at which EPs appear,  $\pm\varepsilon_{\text{EP}}^{\pm} = \pm\sqrt{\gamma(\pm 2t - \gamma)}$ , giving only two EPs at  $\pm\varepsilon_{\text{EP}}^{+(-)}$  for  $\gamma > 0$  ( $\gamma < 0$ ). These EPs connect lines with zero Re energy formed by  $E_0^{\pm}$ , while their Im parts split in a circular fashion between EPs, see Fig. 2(a). This is a remarkable effect of non-Hermiticity on the lowest states, which clearly enforces them to develop a line of zero energy points in stark contrast to the Hermitian regime, where the lowest levels acquire zero energy only at a single point. Unlike the case with  $\varepsilon = 0$ , here  $E_1^{\pm}$  at  $\pm\varepsilon_{\text{EP}}^{\pm}$  remain finite with constant Im parts and energy dependent Re parts which result in a finite gap between the lowest energies and the bulk, see Fig. 2(a). It is also evident from  $\varepsilon_{\text{EP}}^{\pm}$  that larger values of  $t$  make the regions with zero Re part longer. However, while a finite  $\gamma$  is necessary to induce such regions,  $\gamma > 2t$  is detrimental because  $\varepsilon_{\text{EP}}^{\pm}$  becomes Im. In this case, large  $\gamma$  affects the bulk levels  $E_1^{\pm}$  making them to develop EPs as well, see Fig. 2(b).

For  $\varepsilon_L \neq \varepsilon_R$ , the bowtie dependence [47, 48] of the lowest levels with a single zero-energy crossing in the Hermitian regime transforms into a line with zero Re part

and split Im parts with a bubble-like profile under non-Hermiticity [Fig. 2(c)]. Further insight is obtained from Fig. 2(d), where we plot a phase diagram expressed as the Re part of the difference between the lowest electron- and hole-like eigenvalues  $\text{Re}E_{\text{eh}} = \text{Re}(E_0^+ - E_0^-)$ . Here the green region indicates  $\text{Re}E_{\text{eh}} = 0$ , while its borders mark the EPs; the dotted horizontal and vertical lines show  $\text{Re}E_{\text{eh}} = 0$  in the Hermitian regime. A finite non-Hermiticity  $\gamma \neq 0$  induces large regions where the lowest two energy levels become zero modes. In consequence, non-Hermiticity at the sweet spot  $\Delta = t$  offers a much broader range of parameter space to realize PMMMs.

To close this part, we note that, since our system exhibits particle-hole symmetry  $CH^*C^\dagger = -H$ , with  $CC^* = 1$  and  $C = \tau_x \sigma_0$ , the EPs found here are protected by a 0-dimensional  $Z_2$  topological number, which corresponds to the  $D^\dagger$  NH topological class [49].

*Away from the sweet spot  $\Delta \neq t$ .*—Relaxing the ideal sweet spot conditions to  $\Delta \neq t$ , the eigenvalues at  $\varepsilon_{L,R} = \varepsilon$  are still given by Eqs. (3) but now with  $P = t^2 + \Delta^2 + \varepsilon^2 - \gamma^2$  and  $Q = t^2(\Delta^2 - \varepsilon^2) - \varepsilon^2\gamma^2$ . In this case, the eigenvalues develop EPs when  $0 < P \leq \text{Re}(2\sqrt{Q})$  and  $\text{Im}(2\sqrt{Q}) = 0$ , with the equality defining the EP positions as a function of  $t$  given by  $\pm t_{\text{EP}}^\pm = \pm\sqrt{(\Delta \pm \gamma)^2 + \varepsilon^2}$ ; or as a function of the onsite energy  $\pm\varepsilon_{\text{EP}}^\pm = \pm\sqrt{t^2 - (\Delta \pm \gamma)^2}$ . Unlike the sweet spot case, here there can be four EPs at  $\pm t_{\text{EP}}^\pm$  or  $\pm\varepsilon_{\text{EP}}^\pm$ , two at negative and two at positive  $t$  or  $\varepsilon$ , provided  $t > |\Delta \pm \gamma|$  for the latter case. Even for small NH asymmetries  $\gamma$ , the single zero-energy Hermitian crossing at  $t = \Delta$  splits into two EPs  $t_{\text{EP}}^\pm$ , resulting in zero modes for  $t \neq \Delta$ , an effect that occurs for both vanishing and finite  $\varepsilon$ , see Fig. 3(a,b). As noted, the EPs also appear as a function of  $\varepsilon$ , where four EPs form at small  $\gamma$  but, as it gets larger, the EPs closer to  $\varepsilon = 0$  fuse, leaving only the outer EPs connecting lines with zero Re part and circular Im parts  $\text{Im}E_0^\pm \neq 0$ , see Fig. 3(c) and inset therein. The stabilization of  $E_0^\pm$  at zero Re energy by a finite non-Hermiticity is very similar to what we obtain in the sweet spot, but, of course, here no zero energy PMMMs are expected in the Hermitian regime. We note that the zero-energy line between EPs is well separated from the higher energy levels  $E_1^\pm$ , which provides an excitation gap. However, very large non-Hermiticity is not useful because it can force  $E_1^\pm$  to zero Re energy via an EP transition, see Fig. 3(d).

When  $\varepsilon_L \neq \varepsilon_R$ , the formation of zero energy Re lines between EPs in  $E_0^\pm$  remains robust, see Fig. 3(e). At  $\gamma = 0$ , the eigenvalues develop a diamond-like profile which transforms into a line with zero Re energy whose ends mark the EPs, with a bubble-like splitting of the Im parts similar to the sweet spot in Fig. 2(c). The appearance of zero-energy Re lines is a stable effect occurring in a large set of parameters, see Fig. 3(f); the green region indicates  $\text{Re}E_{\text{eh}} = 0$  and its borders signal the position of EPs. We thus conclude that non-Hermiticity has the potential to induce and stabilise zero-energy PMMMs in parameter

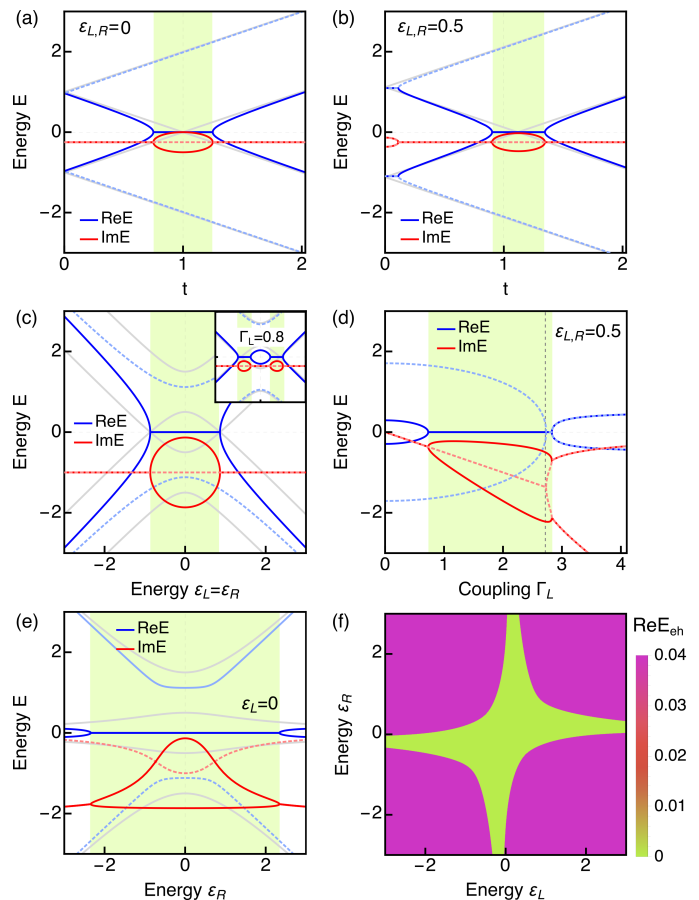


FIG. 3. Re (blue) and Im (red) parts of the eigenvalues away from the sweet spot  $\Delta \neq t$  at finite non-Hermiticity. Panels (a,b) show the eigenvalues as a function of  $t$  for  $\varepsilon_{L,R} = 0$  and  $\varepsilon_{L,R} = 0.5$  at  $\Delta = 1$  and  $\Gamma_L = 0.5$  and  $\Gamma_R = 0$ . (c) shows the eigenvalues as a function of  $\varepsilon_L = \varepsilon_R$  at  $\Gamma_L = 2$  and  $\Gamma_R = 0$ , with the inset at  $\Gamma_L = 0.8$ , while (d) shows the eigenvalues as a function of  $\varepsilon_R$  at  $\varepsilon_L = 0$  at  $\Gamma_L = 2$  and  $\Gamma_R = 0$ . The gray curves in (a-e) correspond to  $\Gamma_{L,R} = 0$ , while the green region ends mark the EPs due to lowest eigenvalues. Vertical dashed line in (e) mark EPs due to higher energy eigenvalues. Panel (f) shows the Re part of the difference between lowest positive and negative eigenvalues  $\text{Re}E_{\text{eh}}$ , where the green region indicates  $\text{Re}E_{\text{eh}} = 0$  and its borders mark the EPs. Parameters: in (c-f)  $\Delta = 0.5$ ,  $t = 1$ ,  $\Gamma_L = 2$ ,  $\Gamma_R = 0$ .

regimes well beyond the Hermitian case.

*Many-body description under non-Hermiticity.*— Further understanding of the role of non-Hermiticity is obtained by inspecting the many-body energies. We thus write  $H_{\text{eff}}$  given by Eq. (2) in the occupation number basis  $|n_L n_R\rangle$ , with  $n_{L,R}$  being the electron number on each QD. Hence,  $\mathcal{H}_{\text{eff}} = \text{diag}(H_e, H_o)$  for the even (e) and odd (o) occupations  $(|00\rangle, |11\rangle, |01\rangle, |10\rangle)$ . Here,  $H_e = (\varepsilon_+ - i\Gamma)(\eta_0 - \eta_z) + \Delta\eta_x$  and  $H_o = (\varepsilon_+ - i\Gamma)\bar{\eta}_0 + (\varepsilon_- - i\gamma)\bar{\eta}_z + t\bar{\eta}_z$ , where  $\varepsilon_\pm = (\varepsilon_L \pm \varepsilon_R)/2$ , and  $\eta_i$  ( $\bar{\eta}_i$ ) is the  $i$ -th Pauli matrix in the even (odd) occupation basis subspace.

The eigenvalues of  $H_{e(o)}$  are then given by

$$\begin{aligned} E_{e,\pm} &= -i\Gamma + \varepsilon_+ \pm \sqrt{\Delta^2 + (\varepsilon_+ - i\Gamma)^2}, \\ E_{o,\pm} &= -i\Gamma + \varepsilon_+ \pm \sqrt{t^2 + (\varepsilon_- - i\gamma)^2}. \end{aligned} \quad (4)$$

As expected, Eqs. (4) reveal that the even sector depends on  $\Delta$  (describing CAR), while the odd sector on  $t$  (describing ECT). A less obvious consequence of coupling this many-body basis to reservoirs is that EPs in the even and odd sectors are governed by  $\Gamma$  and  $\gamma$ , respectively. Specifically, EPs in the even sector form when  $E_{e,\pm}$  merge into a single value, namely, when the square root vanishes,  $\varepsilon_+ = 0$  and  $\Delta^2 = \Gamma^2$ ; even at equal couplings to the leads  $\gamma = 0$ . In contrast, for the odd sector,  $E_{o,\pm}$  merge into a single value when  $\varepsilon_- = 0$  and  $t^2 = \gamma^2$ , thus always requiring  $\gamma \neq 0$ . At  $\varepsilon_{L,R} = 0$ , the EPs of both sectors give zero Re parts and finite Im energies. The EPs discussed here can be seen in Fig. 4(a,b), where we plot  $E_{e(o),\pm}$  as a function of  $\varepsilon_R$  and  $\Gamma_L$ . The even and odd sectors develop EPs at finite non-Hermiticity and they require different amount of  $\Gamma_{L,R}$  away from  $\Delta = t$ .

Having shown the emergence of EPs in the many-body description, a natural question is what happens to the PMMMs discussed in the previous section, namely to the zero-energy excitations between the degenerate even and odd ground states [15], which here can be characterized by  $\text{Re}\delta = \text{Re}(E_{o,-} - E_{e,-}) = 0$ . In the Hermitian regime,  $\Gamma_{L,R} = 0$ , the condition  $\delta = 0$  leads to the sweet spot  $\varepsilon_L \varepsilon_R = t^2 - \Delta^2$ . Under non-Hermiticity,  $\text{Re}\delta = 0$  implies that the sweet spot can be generalized as

$$\begin{aligned} \varepsilon_L \varepsilon_R &= (t^2 - \gamma^2) - (\Delta^2 - \Gamma^2), \\ \Gamma \varepsilon_+ &= \gamma \varepsilon_-. \end{aligned} \quad (5)$$

These conditions imply that, to achieve  $\text{Re}\delta = 0$ , it is necessary that both sectors undergo EP transitions. While this is not immediately obvious from Eqs. (5), a clearer expression for  $\delta$  can be obtained for  $\varepsilon_{L,R} = 0$ , which gives

$$\delta = -\sqrt{t^2 - \gamma^2} + \sqrt{\Delta^2 - \Gamma^2}. \quad (6)$$

The first (second) square root corresponds to the odd (even) sector energy, which, at  $\Delta \neq t$ , host EP transitions at different  $\Gamma_{L,R}$ . Importantly, Eq. (6) reveals that  $\text{Re}\delta = 0$ , associated to the energy of PMMMs, can be only achieved if *both* square roots become Im, which only happens after EP transitions in both sectors. To illustrate this effect, we plot in Fig. 4(c)  $\text{Re}\delta$  as a function of  $\Delta$  and  $t$ . The white color indicates  $\text{Re}\delta = 0$ , which only occurs along a single line  $\Delta = t$  in the Hermitian regime (left panel); this stems from a single point parity crossing of the even and odd energies, see gray lines in Fig. 4(d). Notably, in the non-Hermitian regime,  $\text{Re}\delta = 0$  emerges in a wider region of the  $\Delta - t$  plane (Fig. 4(c), right panel), which here follows from Eq. (6) and reveal that the edges of such white region are determined by

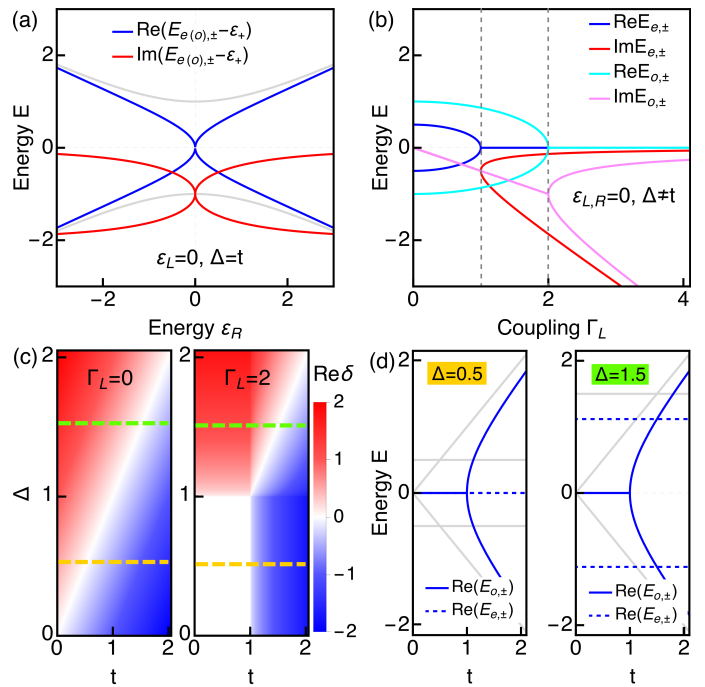


FIG. 4. (a) Re and Im parts of the many-body eigenvalues at finite non-Hermiticity as a function of  $\varepsilon_R$  at  $\Delta = t = 1$ , while (b) as a function of  $\Gamma_L$  at  $\Delta = 0.5$  and  $t = 1$ . Gray curves in (a) are the Hermitian energies; vertical dashed lines in (b) mark the EPs. (c)  $\text{Re}(\delta) = \text{Re}(E_{o,-} - E_{e,-})$  as a function of  $\Delta$  and  $t$  at  $\Gamma_{L/R} = 0$  and  $\Gamma_L = 2, \Gamma_R = 0$ ; here  $\varepsilon_{L,R} = 0$ . White region indicates  $\text{Re}\delta = 0$ . (d) Re parts of the many-body eigenvalues at two fixed values of  $\Delta$  in (c), indicated by orange and green dashed lines. Parameters:  $\Gamma_R = 0$ .

$t \leq \gamma$  and  $\Delta \leq \Gamma$ , with the equality given the EP transitions and the inequality ensuring zero-energy PMMMs.

*Spectral and conductance signatures.*—Having established the stabilization and the realization of zero-energy states by EPs under non-Hermiticity, here we inspect their impact on the spectral function  $A$  and differential conductance  $G_{\alpha\beta} = dI_{\alpha}/dV_{\beta}$ . The former is obtained as  $A(\omega) = -\text{Im}Tr(\mathcal{G}^r - \mathcal{G}^a)$ , where  $\mathcal{G}^r(\omega) = [\mathcal{G}^a(\omega)]^\dagger = (\omega - H_{\text{eff}})^{-1}$  is the retarded Green's function associated to  $H_{\text{eff}}$  given by Eq. (2). The conductance is obtained as  $G_{\alpha\beta}(\omega) = (e^2/h)(\delta_{\alpha\beta} - |S_{ee}^{\alpha\beta}(\omega)|^2 + |S_{he}^{\alpha\beta}(\omega)|^2)$ , where  $S_{ij}^{\alpha\beta}$  are elements of the  $S$ -matrix in Nambu space  $S = 1 - iW^\dagger \mathcal{G}^r(\omega)W$ , with  $W = \text{diag}\{\sqrt{\Gamma_L}, \sqrt{\Gamma_R}, -\sqrt{\Gamma_L}, -\sqrt{\Gamma_R}\}$  characterizing the coupling to the L/R leads.

In Figs. 5 we present  $A$ ,  $G_{RR}$ , and  $G_{RL}$  as a function of  $\varepsilon_L$  at  $\Delta = t$  for distinct couplings to the  $N$  leads and  $\varepsilon = 0.5$ ;  $G_{\alpha\beta}$  is shown in units of  $(e^2/h)$ . The Re and Im part of the eigenvalues is also shown in dashed blue and red curves. The main observation is that these quantities reveal the formation of EPs. The spectral function exhibits large values at low energies, giving rise to two clearly visible branches for positive and negative  $\omega$ , which then merge at the EPs and stick at zero energy, giving

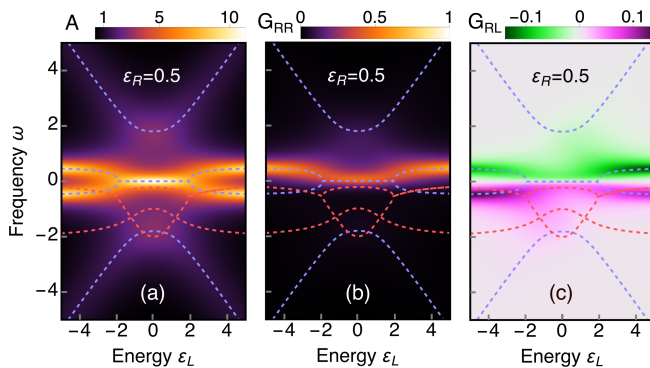


FIG. 5. (a) Spectral function, (b) local conductance, and (c) nonlocal conductance as functions of  $\omega$  and  $\varepsilon_L$  at  $\Delta = t$  and  $\Gamma_L = 2, \Gamma_R = 0.1$ . Parameters:  $\Delta = 1, t = 1, \varepsilon_R = 0.5$ .

rise to large spectral weight between EPs [Fig. 5(a)]. A similar behavior is observed in  $G_{RR}$ , where the positive branch gets to  $\omega = 0$  at the EPs but, in contrast to the case with symmetric  $\Gamma_{L/R}$ , here  $G_{RR}$  is not necessarily quantized due to  $\varepsilon_R \neq 0$ , see Fig. 5(b). When it comes to  $G_{RL}$ , it exhibits positive and negative large values for  $\omega < 0$  and  $\omega > 0$ , whose intensities reduce at the EPs thus making possible the EP detection even though at  $\omega = 0$  the nonlocal conductance vanishes.

In conclusion, we have demonstrated that non-Hermiticity represents a powerful mechanism for stabilizing poor man's Majorana modes in minimal Kitaev chains. In particular, we have considered a two-site Kitaev chain under non-Hermiticity due to coupling to normal leads and discovered that non-Hermiticity induces topologically protected exceptional points, connected by robust zero energy real lines that represent the non-Hermitian realization of the Hermitian poor man's Majorana modes. Our results may help guide the stabilization of poor man's Majorana modes and pave the way for realizing stable non-Hermitian effects by combining few-site Kitaev chains and non-Hermitian topology. Specifically, our findings hold particular relevance for recent experiments, where few-site Kitaev chains have been successfully fabricated [12, 13, 18, 50] and the precise control of couplings to normal leads seems to be feasible [17, 51, 52].

We thank M. Sato and R. Seoane for insightful discussions. J.C. acknowledges financial support from the Swedish Research Council (Vetenskapsrådet Grant No. 2021-04121), the Royal Swedish Academy of Sciences (Grant No. PH2022-0003), and the Carl Trygger's Foundation (Grant No. 22: 2093). R. Aguado acknowledges support from the Horizon Europe Framework Program of the European Commission through the European Innovation Council Pathfinder grant no. 101115315 (QuKiT), the Spanish Ministry of Science through Grants PID2021-125343NB-I00 and TED2021-130292B-C43 funded by MCIN/AEI/10.13039/501100011033, "ERDF A way of making Europe" and European Union

NextGenerationEU/PRTR. Support by the CSIC Interdisciplinary Thematic Platform (PTI+) on Quantum Technologies (PTI-QTEP+) is also acknowledged.

\* jorge.cayao@physics.uu.se

† ramon.aguado@csic.es

- [1] M. Sato and S. Fujimoto, Majorana fermions and topology in superconductors, *J. Phys. Soc. Jpn.* **85**, 072001 (2016).
- [2] M. Sato and Y. Ando, Topological superconductors: a review, *Rep. Prog. Phys.* **80**, 076501 (2017).
- [3] Y. Tanaka, S. Tamura, and J. Cayao, Theory of Majorana zero modes in unconventional superconductors, *Progress of Theoretical and Experimental Physics*, ptae065 (2024).
- [4] S. D. Sarma, M. Freedman, and C. Nayak, Majorana zero modes and topological quantum computation, *npj Quantum Inf.* **1**, 15001 (2015).
- [5] R. Aguado and L. P. Kouwenhoven, Majorana qubits for topological quantum computing, *Physics Today* **73**, 44 (2020).
- [6] C. Beenakker, Search for non-abelian Majorana braiding statistics in superconductors, *SciPost Phys. Lect. Notes*, 15 (2020).
- [7] Y. Oreg, G. Refael, and F. von Oppen, Helical Liquids and Majorana Bound States in Quantum Wires, *Phys. Rev. Lett.* **105**, 177002 (2010).
- [8] R. M. Lutchyn, J. D. Sau, and S. Das Sarma, Majorana fermions and a topological phase transition in semiconductor-superconductor heterostructures, *Phys. Rev. Lett.* **105**, 077001 (2010).
- [9] R. Aguado, *La Rivista del Nuovo Cimento* **40**, 523 (2017).
- [10] R. M. Lutchyn, E. P. A. M. Bakkers, L. P. Kouwenhoven, P. Krogstrup, C. M. Marcus, and Y. Oreg, *Nat. Rev. Mater.* **3**, 52 (2018).
- [11] E. Prada, P. San-Jose, M. W. A. de Moor, A. Geresdi, E. J. H. Lee, J. Klinovaja, D. Loss, J. Nygård, R. Aguado, and L. P. Kouwenhoven, From Andreev to Majorana bound states in hybrid superconductor-semiconductor nanowires, *Nat. Rev. Phys.* **2**, 575 (2020).
- [12] T. Dvir, G. Wang, N. van Loo, C.-X. Liu, G. P. Mazur, A. Bordin, S. L. Ten Haaf, J.-Y. Wang, D. van Driel, F. Zatelli, *et al.*, Realization of a minimal Kitaev chain in coupled quantum dots, *Nature* **614**, 445 (2023).
- [13] S. L. D. ten Haaf, Q. Wang, A. M. Bozkurt, C.-X. Liu, I. Kulesh, P. Kim, D. Xiao, C. Thomas, M. J. Manfra, T. Dvir, M. Wimmer, and S. Goswami, A two-site Kitaev chain in a two-dimensional electron gas, *Nature* **630**, 329 (2024).
- [14] A. Y. Kitaev, Unpaired Majorana fermions in quantum wires, *Physics-Uspekhi* **44**, 131 (2001).
- [15] M. Leijnse and K. Flensberg, Parity qubits and poor man's Majorana bound states in double quantum dots, *Phys. Rev. B* **86**, 134528 (2012).
- [16] J. D. Sau and S. D. Sarma, Realizing a robust practical Majorana chain in a quantum-dot-superconductor linear array, *Nat. Commun.* **3**, 964 (2012).
- [17] A. Bordin, G. Wang, C.-X. Liu, S. L. D. ten Haaf, N. van Loo, G. P. Mazur, D. Xu, D. van Driel, F. Za-

- telli, S. Gazibegovic, G. Badawy, E. P. A. M. Bakkers, M. Wimmer, L. P. Kouwenhoven, and T. Dvir, Tunable crossed Andreev reflection and elastic cotunneling in hybrid nanowires, *Phys. Rev. X* **13**, 031031 (2023).
- [18] F. Zatelli, D. van Driel, D. Xu, G. Wang, C.-X. Liu, A. Bordin, B. Roovers, G. P. Mazur, N. van Loo, J. C. Wolff, A. M. Bozkurt, G. Badawy, S. Gazibegovic, E. P. A. M. Bakkers, M. Wimmer, L. P. Kouwenhoven, and T. Dvir, Robust poor man's Majorana zero modes using Yu-Shiba-Rusinov states, arXiv: 2311.03193 (2023).
- [19] G. Wang, T. Dvir, G. P. Mazur, C.-X. Liu, N. van Loo, S. L. D. ten Haaf, A. Bordin, S. Gazibegovic, G. Badawy, E. P. A. M. Bakkers, M. Wimmer, and L. P. Kouwenhoven, Singlet and triplet Cooper pair splitting in hybrid superconducting nanowires, *Nature* **612**, 448 (2022).
- [20] A. Bordoloi, V. Zannier, L. Sorba, C. Schönenberger, and A. Baumgartner, Spin cross-correlation experiments in an electron entangler, *Nature* **612**, 454 (2022).
- [21] Q. Wang, S. L. D. ten Haaf, I. Kulesh, D. Xiao, C. Thomas, M. J. Manfra, and S. Goswami, Triplet correlations in cooper pair splitters realized in a two-dimensional electron gas, *Nat. Commun.* **14**, 4876 (2023).
- [22] N. Moiseyev, *Non-Hermitian Quantum Mechanics* (Cambridge University Press, 2011).
- [23] Y. Ashida, Z. Gong, and M. Ueda, Non-Hermitian physics, *Adv. Phys.* **69**, 249 (2020).
- [24] S. Datta, *Electronic transport in mesoscopic systems* (Cambridge university press, 1997).
- [25] E. J. Bergholtz, J. C. Budich, and F. K. Kunst, Exceptional topology of non-Hermitian systems, *Rev. Mod. Phys.* **93**, 015005 (2021).
- [26] N. Okuma and M. Sato, Non-Hermitian topological phenomena: a review, *Annu. Rev. Condens. Matter Phys.* , **83** (2023).
- [27] J. Cayao and M. Sato, Non-hermitian phase-biased Josephson junctions, arXiv:2307.15472 (2023).
- [28] C.-A. Li, H.-P. Sun, and B. Trauzettel, Anomalous Andreev spectrum and transport in non-Hermitian Josephson junctions, arXiv:2307.04789 (2024).
- [29] P.-X. Shen, Z. Lu, J. L. Lado, and M. Trif, Non-Hermitian persistent current transport, arXiv:2403.09569 (2024).
- [30] C. W. J. Beenakker, Josephson effect in a junction coupled to an electron reservoir, arXiv:2404.13976 (2024).
- [31] D. M. Pino, Y. Meir, and R. Aguado, Thermodynamics of non-Hermitian Josephson junctions with exceptional points, arXiv:2405.02387 (2024).
- [32] Z. Gong, Y. Ashida, K. Kawabata, K. Takasan, S. Hishikawa, and M. Ueda, Topological phases of non-Hermitian systems, *Phys. Rev. X* **8**, 031079 (2018).
- [33] K. Kawabata, K. Shiozaki, M. Ueda, and M. Sato, Symmetry and topology in non-Hermitian physics, *Phys. Rev. X* **9**, 041015 (2019).
- [34] D. I. Pikulin and Y. V. Nazarov, Topological properties of superconducting junctions, *JETP Lett.* **94**, 693 (2012).
- [35] P. A. Iosevich and M. V. Feigel'man, Tunneling conductance due to a discrete spectrum of Andreev states, *New J. Phys.* **15**, 055011 (2013).
- [36] P. San-José, J. Cayao, E. Prada, and R. Aguado, Majorana bound states from exceptional points in non-topological superconductors, *Sci. Rep.* **6**, 21427 (2016).
- [37] J. Avila, F. Peñaranda, E. Prada, P. San-Jose, and R. Aguado, Non-Hermitian topology as a unifying framework for the Andreev versus Majorana states controversy, *Communications Physics* **2**, 133 (2019).
- [38] E. J. Bergholtz and J. C. Budich, Non-Hermitian Weyl physics in topological insulator ferromagnet junctions, *Phys. Rev. Research* **1**, 012003 (2019).
- [39] J. Cayao and A. M. Black-Schaffer, Exceptional odd-frequency pairing in non-Hermitian superconducting systems, *Phys. Rev. B* **105**, 094502 (2022).
- [40] R. Mélin, Multiterminal ballistic Josephson junctions coupled to normal leads, *Phys. Rev. B* **105**, 155418 (2022).
- [41] M. A. Javed, J. Schwibbert, and R.-P. Riwar, Fractional Josephson effect versus fractional charge in superconducting-normal metal hybrid circuits, *Phys. Rev. B* **107**, 035408 (2023).
- [42] J. Cayao and A. M. Black-Schaffer, Bulk Bogoliubov Fermi arcs in non-Hermitian superconducting systems, *Phys. Rev. B* **107**, 104515 (2023).
- [43] J. Cayao, Exceptional degeneracies in non-Hermitian Rashba semiconductors, *J. Condens. Matter Phys.* **35**, 254002 (2023).
- [44] P. Kokhanchik, D. Solnyshkov, and G. Malpuech, Non-Hermitian skin effect induced by Rashba-Dresselhaus spin-orbit coupling, *Phys. Rev. B* **108**, L041403 (2023).
- [45] J. Cayao, Non-Hermitian zero-energy pinning of Andreev and Majorana bound states in superconductor-semiconductor systems, arXiv:2404.11026 (2024).
- [46] We also note that the wavefunctions associated to these levels with zero Re part are well localized at each QD, in a similar fashion as in the Hermitian regime [15].
- [47] E. Prada, R. Aguado, and P. San-Jose, Measuring Majorana nonlocality and spin structure with a quantum dot, *Phys. Rev. B* **96**, 085418 (2017).
- [48] R. S. Souto, A. Tsintzis, M. Leijnse, and J. Danon, Probing Majorana localization in minimal Kitaev chains through a quantum dot, *Phys. Rev. Res.* **5**, 043182 (2023).
- [49] K. Kawabata, T. Bessho, and M. Sato, Classification of exceptional points and non-Hermitian topological semimetals, *Phys. Rev. Lett.* **123**, 066405 (2019).
- [50] A. Bordin, X. Li, D. van Driel, J. C. Wolff, Q. Wang, S. L. D. ten Haaf, G. Wang, N. van Loo, L. P. Kouwenhoven, and T. Dvir, Crossed Andreev reflection and elastic co-tunneling in a three-site Kitaev chain nanowire device, arXiv:2306.07696 (2023).
- [51] Y. Chen, D. van Driel, C. Lampadaris, S. A. Khan, K. Alattallah, L. Zeng, E. Olsson, T. Dvir, P. Krogstrup, and Y. Liu, Gate-tunable superconductivity in hybrid InSb-Pb nanowires, *Appl. Phys. Lett.* **123**, 082601 (2023).
- [52] G. Wang, T. Dvir, G. P. Mazur, C.-X. Liu, N. van Loo, S. L. Ten Haaf, A. Bordin, S. Gazibegovic, G. Badawy, E. P. Bakkers, *et al.*, Singlet and triplet cooper pair splitting in hybrid superconducting nanowires, *Nature* **612**, 448 (2022).